ZIBELINE INTERNATIONAL™ PUBLISHING

ISSN: 2576-6724 (Print)
ISSN: 2576-6732 (Online)
CODEN: ACMCCG

Acta Chemica Malaysia (ACMY)

DOI: http://doi.org/10.26480/acmy.01.2024.51.61

RESEARCH ARTICLE

THE EFFECT OF HYDROXYL SUBSTITUENTS' POSITION ON QUINOLINE IN THE INHIBITION OF ALUMINIUM CORROSION IN HYDROCHLORIC ACID

A.M. Usman[*a], A.A.Muhammad[*b], Jaweria Ambreen[*c,d], Syafiqah Saidin[d] , N.U. Shehu[b], and Otaru Fatimat Oyiza[a]

[a]Department of Chemistry Federal College of Education (Technical) Bichi, P.M.B.3473, Kano, Nigeria
[b]Department of Pure and Industrial Chemistry Bayero University, P.M.B. 3011, Kano. Nigeria.
[c]Department of Chemistry COMSATS University Islamabad, Park road, 45550, Islamabad, Pakistan
[d]Department of biomedical engineering, & Health Sciences, Faculty of Electrical Engineering, University teknologi Malasiya, 81310 UTM , Johor bahru, Malasiya
**Corresponding Author Email: amusman.se@fcetbichi.edu.ng.*

ARTICLE DETAILS

Article History:

Received 23 June 2024
Revised 15 July 2024
Accepted 19 August 2024
Available online 21 August 2024

ABSTRACT

The ability of several hydroxyquinolines to inhibit aluminum corrosion and the effect of hydroxyls at 6, 7, and 8 positions on quinolines in hydrochloric acid were experimentally studied by weight loss, EIS, and PDP. To promote weight loss, 6-hydroxyquinoline (6-OHQ), 7-hydroxyquinoline (7-OHQ), and 8-hydroxyquinoline (8-OHQ) were used under different mass and temperature conditions at different HCl concentrations. The adsorption properties of these inhibitors proved to be reliable. Both chemical and physical mechanisms were significant in the Longmuir isotherm. In comparison, 7-hydroxyquinoline performed better than 6-hydroxyquinoline in terms of corrosion inhibition percentage, mass loss, inhibition efficiency, and surface coverage measured by weight loss. Under identical conditions, 8-hydroxyquinoline performed the worst in terms of corrosion inhibition. The inhibition process proceeded more rapidly in each system via first order kinetics. The surface morphology and functional groups were examined by SEM and FTIR before and after the corrosion study. The weight loss and Nyquist plots from the impedance data and parameters both showed the same behavior. The Tafel plot parameters and polarization data both show the same trend. The EIS, PDP, and weight reduction results are relatively consistent. Although each molecule exhibited excellent corrosion inhibition performance, the 7-OHQ molecule is superior to the other two molecules in inhibiting aluminum corrosion.

KEYWORDS

HydroxyQuinoline, aluminium, corrosion, substituent, position, inhibition, performance

1. INTRODUCTION

In general, the study of the anticorrosive effect of some organic particles and their compounds on metals is the subject of research aimed at developing effective inhibitors based on the properties and environment of the metals (Abdallah, 2002; Ali et al., 2023). Thus, various types of organic inhibitors have been the subject of intensive research as materials for protecting the surfaces of ferrous and non-ferrous metals and their alloys from corrosion and aggressive conditions (Awad, 2004; Babic-Samardz ˇija and Hackerman, 2006). Like iron, aluminum is widely used throughout the world and is the least valuable metal among non-ferrous metals. Under completely different conditions, it is very sensitive to all forms of corrosion. Although aluminum is relatively weak in neutral water, it is very susceptible to corrosion in weakly acidic environments such as corrosive water (Babic´ Samardz˘ija and 2005a). The resistance of aluminum and its oxides to the destructive effects of chloride particles in aqueous media has been extensively studied (Chi and Zhao 2009). The effectiveness of organic inhibitors depends on the size of the organic atoms, aromaticity, the type and number of bonding groups (π and σ bonds) on or in the molecule, the characteristics and surface charge, the charge distribution in the molecule, and the type of positive medium (Cicek, and Al-Numan, 2011; Dai and Zhang, 2012). The presence of polar beneficial groups containing S-, O-, or N-iota, heterocyclic compounds in the molecule, and the proximity of pi-electron reflectors also enhance the effectiveness of these organic corrosion inhibitors (Dai and Zhang, 2012).

The use of computational chemistry such as density functional theory (DFT), atomic element simulation (MD), Monte Carlo simulation (MC), and quantitative structure-activity relationship modeling (QSAR) have been used to study the anticorrosive properties of organic materials and molecules. The aromatic ring is generally considered to be the location where some inhibitors can prevent metal corrosion (Dai and Zhang, 2012). Existing studies on corrosion inhibition by quinoline atoms focus on the nature and type of functional groups (substituted or not) attached to the molecules used (Dakeshwar et al., 2021). To the best of our knowledge, the influence of the position of the substituent on the erosion resistance ability of aluminum in an acidic environment is usually the main factor. The erosion inhibition effect of heterocyclic compounds can also be affected by the type and position of the substituents attached to the particles, in addition to aromaticity, functional groups, and the type of substituents (Eddy et al., 2009). Hydroxyquinoline is a bicyclic heterocyclic nitrogen compound with the molecular formula C9H7NO, which is said to have a good corrosion inhibition effect on metals because it bonds with high electron density (10-π and two non-bonding electrons). Quinoline derivatives with polar substituents such as hydroxyl (-OH) can effectively adsorb through coordinate bonds and form very stable chelate complexes with metal atoms on the surface. Existing studies on corrosion inhibition by quinoline molecules focus on the nature and type of functional groups (substituted or not) attached to the molecules used (EI-Awady et al., 1994).

Quick Response Code	Access this article online	
	Website: www.actachemicamalaysia.com	DOI: 10.26480/acmy.01.2024.51.61

Cite the Article: A.M. Usman, A.A.Muhammad, Jaweria Ambreen, Syafiqah Saidin , N.U. Shehu, and Otaru Fatimat Oyiza (2024). The Effect of Hydroxyl Substituents' Position on Quinoline in The Inhibition of Aluminium Corrosion In Hydrochloric Acid. *Acta Chemica Malaysia, 8(1): 51-61.*

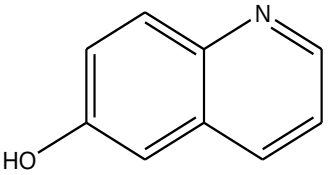

Figure 1: 6-hydroxyquinoline

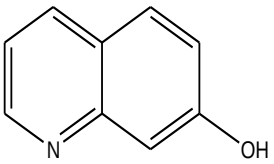

Figure 2: 7-hydroxyquinoline

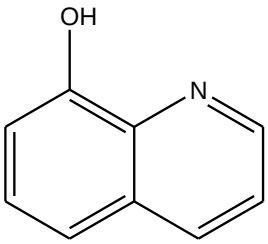

Figure 3: 8-hydroxyquinoline

2. MATERIALS AND METHODS

2.1 Materials

The inhibitors are three quinoline derivatives (6,7- and 8-hydroxyquinoline) from Aldrich Chemical Co.Ltd. (Gillingham, Dorset, UK), all of which are 99% pure. They were used without further washing. Other components include distilled water, ethanol; hydrochloric acid, 96% pure; diethyl ether, 37% pure, specific gravity 1.175-1.185 g/20 °C; 99.5% pure, specific gravity 0.713-0.714. The aluminum sheets used in this study are wrought type aluminum composed of 98.9% Al, 0.5% and 0.48% Si with trace amounts of other elements such as Ti, V, Mn, Ni, Cu, and Ga. The metal coupons used in this experiment were machine cut and optimized (5.0 cm × 3.0 cm × 0.11 cm), degreased with ethanol, rinsed with acetone, air dried, and stored in a moisture-free desiccator prior to corrosion studies.Calibration test solutions were prepared by diluting 37% HCl from Sigma-Aldrich with double-distilled water (EI-Awady et al., 1994).

2.2 Mass Loss Measurement

The Metals coupons (5.0 cm × 3.0 cm × 0.11 cm) were obtained and firstly weighed, suspended with the aid of Pyrex glass hooks tightened on a rod horizontally placed on two pairs of retort stands so that 4.0cm × 3.0cm of the metal to study was immersed each in 80ml of 0.2M, 0.4M and 0.6M HCl solutions respectively, containing different concentration of inhibitor at 0.0, 0.2, 0.4, and 0.6 g/L . Contact time was allowed for five hour for (5h) at 303, 313 and 323K. The aluminium samples (coupons) were then withdrawn at predetermined intervals of time, washed, rinsed in diethyl ether, dried and reweighed. The mass losses was recorded. Through above procedure coupons were tested for all the three quinoline derivatives. Each experiment was carried out three times (Ekanem et al., 2010). The mass measurements was carriedout on Mettler FA2004 electronic balance. From the mass loss data, corrosion rate (CR, in $gh^{-1}cm^{-2}$), the degree of surface coverage (θ) and Inhibition efficiency I (%) were computed using Equations (Elfaydy et al., 2016):

$$\text{Weight Loss} = W_1 - W_2 \quad (1)$$

$$\theta = 1 - \frac{W_1}{W_2} \quad (2)$$

$$\%\ IE = \left(1 - \frac{W_1}{W_2}\right) \times 100 \quad (3)$$

$$CR\ (gh^{-1}cm^{-2}) = \frac{\Delta W}{At} \quad (4)$$

W_1 is the initial masses (g) of Al and W_2 is the final mass after time t, θ is the degree of surface coverage of the inhibitor, A is the area of the Al coupon (cm2), t is the immersion time (h).

2.3 Electrochemical Measurements

2.3.1 Impedance Measurement

The Impedance measurement was carried out at 303 ± 1K in a three cathode cell utilizing a Gamry interface 5000E potentiostat (Louis Drive Warminster, Father 18974, USA) arranged with add up to Gamry frameworkversion 7.9.0 and Gamry Ecchm Agent version7.9.0 , with V3 Studio computer program over a repeat expand of 100 kHz - 10 mHz, with a hail adequacy of 5mV. A graphite bar was utilized as counter cathode and Ag/AgCl terminal was utilized as the reference cathode. The final specified was related through a Luggin's capillary. Estimations was performed in circulated discuss through and unstirred courses of action after 30 minutes immersion inside the test courses of action. The working electrode was prepared from square sheets of aluminum with $1cm^2$ of the locale revealed to the test course of action (El-HassanAssiri et al., 2020). Starting lab program was utilized for the data managing with which gives the Nyquest plot of each system. The charge trade resistance values were gotten from the breadth of the semi circles of the Nyquist plots. The obstacle efficiencies of the inhibitors was additionally calculated from the charge trade resistance values (Kadapparambil et al., 2017).

2.3.2 Potentiodynamic Polarization

The polarization studies were carried out using a complete Gamry framework version 7.9.0, an acquisition system with NOVA installed, software package version 1.8, and an electrochemical three-electrode cell with a metal coupon of surface 1 cm^2 as working electrode, an Ag/AgCl reference electrode, and a graphite counter electrode. The dimensions of the aluminum samples for the electrochemical experiments were 1.0 cm × 1.0 cm × 0.11 cm. They were then encapsulated with epoxy resin such that only a square surface of 1.0 cm2 in area was left uncovered. The exposed surfaces were degreased with acetone, rinsed with distilled water, and air-dried. The aluminum metal was polarized between -1,000 and 2,000 mV at 303 K with a specific scan rate of 0.333 mV s-1. From the polarization test data of inhibited aluminum in acidic media, electrochemical parameters such as Tafel slope, corrosion potential, corrosion current and corrosion rate were calculated. The linear regions of the anodic and cathodic curves were extrapolated at a scan rate of 0.0016 V/s. From the Tafel analysis, the corrosion current density, corrosion rate, linear polarization resistance and corrosion potential in static solution were determined (Kadapparambil et al., 2017). The inhibition efficiency IU (%) was also calculated. Each test was performed in triplicate. The measurements were carried out in 0.4 M acid solution containing 0.4 g/l mass of the tested inhibitor. The inhibition efficiency (%IE) was derived from the linear polarization resistance (LPR) and potentiodynamic polarization corrosion rate (PP-CR), which were used as a criterion to evaluate the corrosion resistance of aluminum in corrosive environments using the following equation:

$$\%IE = \frac{CR_o - CR}{CR_o} \times 100 \quad (5)$$

Where $CR_o$and CR are corrosion rates of the materials in the presence and absence of inhibitors respectivel (Khaled and Abdel Shafi, 2011).

2.4 Surface Characterization

To understand the type and nature of aluminum corrosion, the resulting surfaces were examined before and after corrosion using a Phenom ProX (Netherlands) scanning electron microscope at an accelerating voltage of 5.00 kV. Infrared spectra of the adsorbed inhibitors were recorded over the frequency range of 400-4000 cm-1 using a SHIMADZU FTIR-8400S Fourier transform infrared spectrometer (FTIR). To ascertain the purity of the aluminium test plate, Elemental was performed using a MiniPal 4 PW4030 Energy Dispersive X-ray Fluorescence Spectrometer (EDXRF) with Mini Pal analysis software installed. The samples were stimulated with a potential of 30 kV and a current of 1 mA for 10 min.

3. Results and Discussion

3.1 Weight Loss Analysis

The corrosion performance profiles of 6-OHQ, 7OHQ and 8-OHQ systems in terms of the corrosion inhibition effect on aluminium by weight loss tests are shown in Figures 3.1 to 3.5 below. The profiles starting from Figure 3.1 show the results of all three systems (6-OHQ/0.2 MHCl on Al, 7-OHQ/0.2 MHCl on Al, 8-OHQ/0.2 MHCl on Al) treated simultaneously under the same conditions. The vertical height of the bars in Figures 3.1 to 3.3 is a function of the total weight loss of aluminium in the tests of the transparent and inhibited cases for all systems. This is related to the fact that in many cases the close proximity of inhibitor particles prevents the corrosive (destructive) particles from making full contact with the metal surface, forming a boundary between the particles, which can be physical or chemical depending on the adsorption characteristics (Kiani et al., 2008). It can be imagined as follows: without the inhibitor, the metal surface is like a smooth and flat surface. When a rust particle strikes a metal surface, it must overcome a certain resistance to pass through the surface and initiate the corrosion reaction. However, when an inhibitor is released, it behaves like a small bump on the metal surface. Thanks to the inhibitor molecules, the rust particle can now be better removed from the metal surface. In this case, the rust particle does not have to overcome as much resistance to initiate the corrosion reaction. Thus, the closer the inhibitor molecules are, the lower the activation strength required for the reaction. The change in inhibitor mass from 0.0 to 0.2, 0.4 to 0.6 g/l shown in Figures 4 to 6 leads to a decrease in the mass hardness of aluminum at all temperatures and all rust concentrations. Typically, increasing the inhibitor mass increases the number of inhibitor ions that can access the rust atoms, making them less irritating -- it's like putting more bumpers on a metal surface to make it easier for rust particles to stick to.

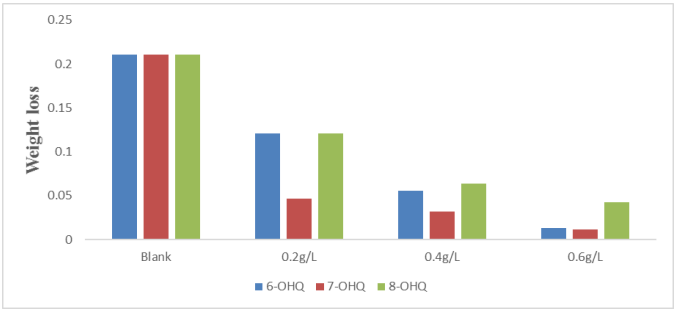

Figure 4: Weight loss of aluminium in 0.2M HCl at 303k using inhibitors 6-OHQ, 7-OHQ and 8-OHQ with varying massX for each system.

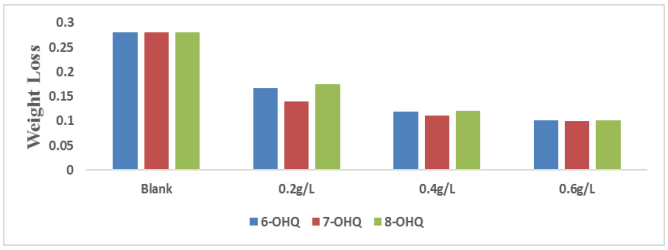

Figure 5: Weight loss of aluminium in 0.2M HCl at 313k using inhibitors 6-OHQ, 7-OHQ and 8-OHQ with varying mass for each system.

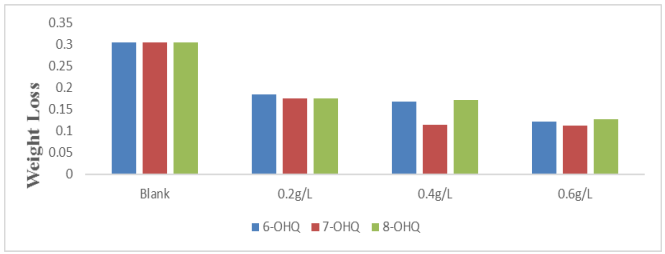

Figure 6: Weight loss of aluminium in 0.2M HCl at 323k using inhibitors 6-OHQ, 7-OHQ and 8-OHQ with varying mass for each system.

Moreover, Figures 4 to 6 show clear examples of the effects of temperature variations up to 303 K, 313 K, and 323 K. As the temperature increases, the mass loss of the metal increases. This has been explained by many scientists (Kikuchi, 1987). This is because at high temperatures the inhibitor atoms on the metal surface become insulating and more permeable. This allows multiple contacts between the metal and the oxide atoms, resulting in a larger mass loss than at room temperature (Kliskic et al., 2000). Another noteworthy effect from Figures 4 to 6 is that 7-OHQ has the lowest mass loss (shortest bar) relative to the total inhibitor mass at all temperatures. This is a clear indication that 7-OHQ is more strongly adsorbed on the metal surface than the other inhibitors. Thus, despite the relative inhibitor measurements, 7-OHQ shows a comparatively lower mass loss than 6-OHQ and 8-OHQ, clearly indicating its superior corrosion inhibition effect.

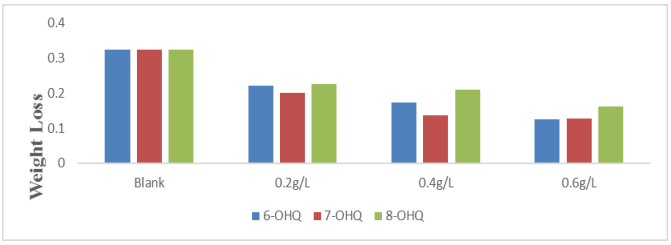

Figure 7: Weight loss of aluminium in 0.4M HCl at 303k using inhibitors 6-OHQ, 7-OHQ and 8-OHQ with varying mass for each system.

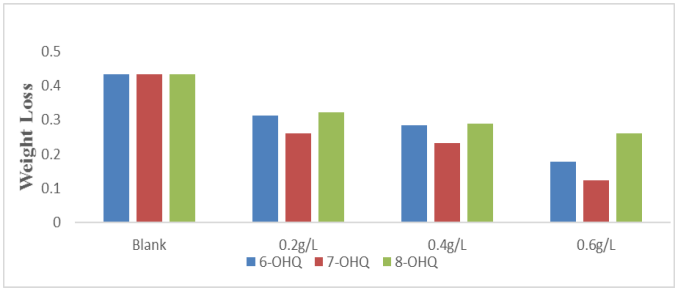

Figure 8: Weight loss of aluminium in 0.6M HCl at 303k using inhibitors 6-OHQ, 7-OHQ and 8-OHQ with varying mass for each system.

Figures 6 to 8 show the increase in inhibitor concentration over the range of increasing metal mass loss, independent of temperature and inhibitor mass. Corrosion is faster at 0.6M, then 0.4M, then 0.2M, and metal corrosion is lower at all temperatures with or without inhibitor. This is due to the decomposition of the passive film formed by the discussion and the occurrence of pinning corrosion, which is usually followed by a stable corrosion state due to the cathodic reaction (Larif et al., 2013). In most cases, the reason for changing the inhibitor concentration in corrosion protection studies is to be able to observe how the adsorption behavior changes with the corrosion resistance of the environment. It is also useful to determine the optimal inhibitor concentration for a given level of corrosion. As the inhibitor concentration increases, the activation energy of the reaction decreases. This is often because there are more destructive particles available for the reaction, providing more energy to initiate the reaction beyond the energy limit (Li et al., 2019).

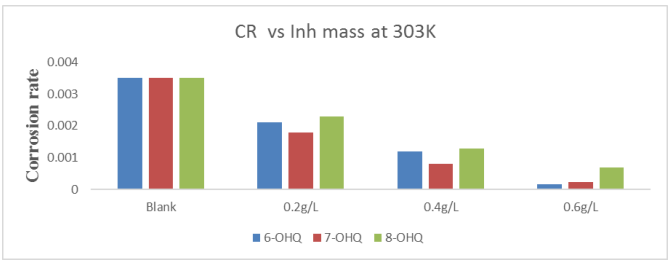

Figure 9: Corrosion Rate of aluminium in 0.2M HCl at 303k with varying inhibitor mass for each system.

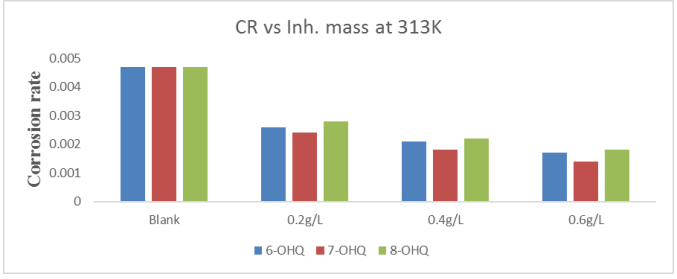

Figure 10: Corrosion Rate of aluminium in 0.2M HCl at 313K with varying inhibitor mass for each system.

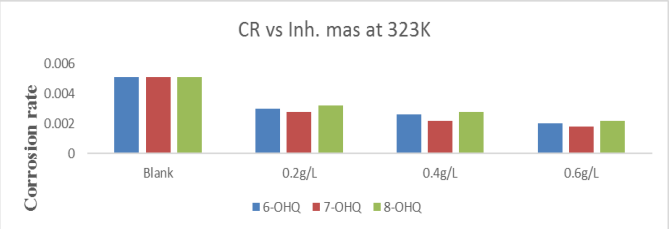

Figure 11: Corrosion Rate of aluminium in 0.2M HCl at 323k with varying inhibitor mass for each system.

3.2 Corrosion Rate Analysis

Corrosion rate is a measure of how quickly a material is eroded or immersed in a corrosive solution (Li et al., 2019). It can be expressed as the amount of material lost over time, for example, milligrams per square meter per day. The erosion rate is an important factor to consider when studying erosion inhibition, since the common goal is to reduce the erosion rate (Moussa et al., 1988). Figures 9, 10 and 11 are plots of the erosion rate in 0.2 MCl at temperatures of 303 K, 313 K, and 323 K, respectively, with different amounts of inhibitor for each system. From the data above, we can see that as the temperature increases, the overall erosion rate for all systems also increases; however, the attack rate is slower near the inhibitor. As the concentration of corrosion inhibitor increases, the corrosion rate tends to decrease. In fact, the inhibitor atoms adsorbed on the metal surface form a protective layer that prevents the metal from being exposed to destructive conditions.The more inhibitor particles there are, the thicker the protective layer and the slower the corrosion rate. The numbers 9, 10 and 11 all indicate slower corrosion rates, with 7-OHQ being the inhibitor with the shorter bar. It was observed that 7-OHQ is more strongly attracted to the metal surface than the other inhibitors used here. In this study, the corrosion rates are in the order 8-OHQ > 6-OHQ > 7-OHQ. Although these particles have the same atomic weight and the same iota number, there is a significant difference in their effectiveness in reducing the corrosion rate.

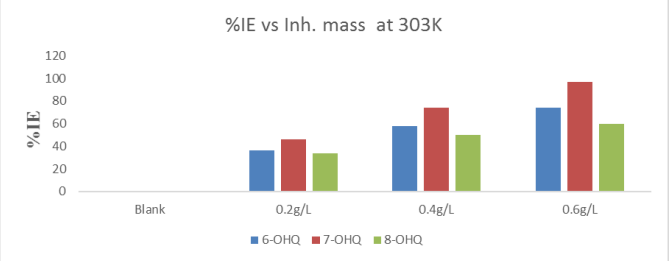

Figure 12: %IE for corrosion of aluminium in 0.2M HCl at 303k with varying inhibitor mass for each system.

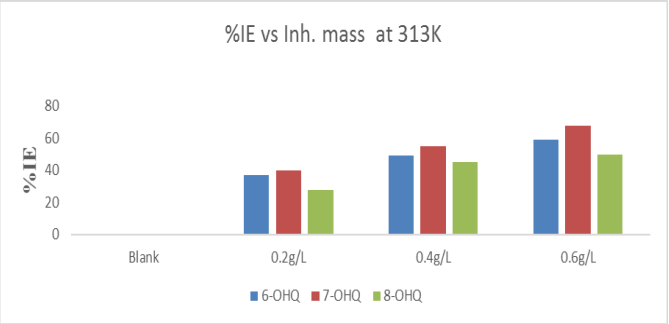

Figure 13: %IE for corrosion of aluminium in 0.2M HCl at 313k with varying inhibitor mass for each system.

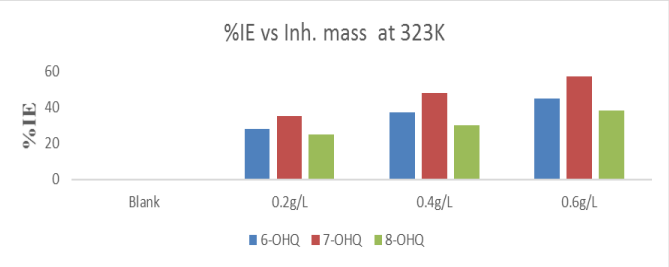

Figure 14: %IE for corrosion of aluminium in 0.2M HCl at 323k with varying inhibitor mass for each system.

Figures 12, 13 and 14 are the rate inhibition efficiency (%IE) profiles in 0.2 M HCl at 303 K, 313 K, and 323 K, respectively, with different inhibitor masses for each system. The inhibition efficiency of a particular particle is the percentage decrease in erosion rate when an erosion inhibitor is added (Murulana et al., 2012). The figures above show that the vertical height of the bars increases with increasing inhibitor mass for each inhibitor, which indicates that the rate inhibition efficiency increases coordinately with increasing inhibitor mass at all temperatures. Again, unlike weight loss and erosion rate, the rate inhibition efficiency increases with increasing inhibitor mass and decreases with increasing temperature. Although the three molecules used here (6-OHQ, 7-OHQ, and 8-OHQ) have almost the same atomic weight and molecular number, it is clear that the 7-OHQ molecule has the highest rate-limiting efficiency, followed by 6-OHQ and 8-OHQ, and the lowest. This can also be seen from Table 1, which shows the mass numbers of the inhibitors in 0.2 M HCl versus temperature. Both the mass loss and rate-limiting efficiency values are consistent with the figures given above. There are possible reasons for the differences in loss rates and rate-confining efficiencies among the three atoms, which can be investigated here after considering other experimental results (PDP and EIS) and quantum chemical parameters.

Table 1: Mass loss of the aluminium and the inhibition efficiency of each inhibitor using masses of 0.2g, 0.4g and 0.6g in 0.2M Hydrochloric Acid (Corrodent) at 303k, 313k and 323k

S/N	Inhibitor	Conc. g/L	Average mass loss (g) at 303k	%IE	Average mass loss (g) at 313k	%IE	Average mass loss (g) at 323k	%IE
	Blank	0	0.2110	0	0.2810	0	0.3061	0
1	6-OHQ	0.2	0.1210	46	0.1710	37	0.1854	32
		0.4	0.0602	61	0.1212	47	0.1685	45
		0.6	0.0227	85	0.1014	54	0.1220	52
2	7-OHQ	0.2	0.1197	48	0.1673	41	0.1764	38
		0.4	0.0512	74	0.1201	58	0.1585	55
		0.6	0.0114	97	0.1020	66	0.1174	63
3	8-OHQ	0.2	0.1306	34	0.1761	32	0.1914	30
		0.4	0.0637	52	0.1215	43	0.1732	39
		0.6	0.0428	65	0.1079	50	0.1281	48

Table 1 clearly shows the increase in mass loss with increasing temperature, the decrease in mass loss with increasing inhibitor concentration, and the increase in rate inhibition efficiency, which have been described in detail by various researchers (Olufunmilayo and Olakunle, 2020). From the parameters in the table, under the same conditions, 7-OHQ has a better inhibition performance, followed by 6-OHQ and 8-OHQ. However, overall, all particle representations differ especially in terms of the decay limit for aluminum in HCl environment. The specific objective of using corrosion inhibitors is to avoid or minimize to reasonable levels the extreme chemical attack on metal surfaces that results in economic and social consequences (Qiang et al., 2018).

3.3 kinetic Study

Table 2: Kinetics for Corrosion of aluminium using 0.4g s of each inhibitor in 0.4M Hydrochloric Acid (Corrodent) at varying temperature.

Inhibitor			6-OHQ			
Temp.	303K		313K		323K	
1st order	k_1	R^2	k_1	R^2	k_1	R^2
2nd order	0.018	0.999	0.022	0.998	0.025	0.997
	0.001	0.542	0.004	0.239	0.005	0.498

Inhibitor			7-OHQ			
Temp.	303K		313K		323K	
1st order	k_1	R^2	k_1	R^2	k_1	R^2
2nd order	0.016	0.999	0.020	0.999	0.024	0.998
	0.001	0.352	0.003	0.697	0.005	0.696

Inhibitor			8-OHQ			
Temp.	303K		313K		323K	
8-OHQ	k_1	R^2	k_1	R^2	k_1	R^2
1st order	0.016	0.997	0.021	0.998	0.022	0.999
2nd order	0.001	0.342	0.003	0.568	0.004	0.698

Table 2 presented details of the kinetic parameters obtained from weight loss experiments for aluminium corrosion in HCl solutions using hydroxyquinolines at different temperatures. The value of the rate constant and the R-square value are the parameters for establishing the kinetics of chemical reaction at varying temperature (Hamadi et al., 2018). R-square values are more close to unity in most of the systems for the first order results than that of the second order, and also higher values of the rate constant. This confirmed the fact that the corrosion inhibition of alumunium with hydroxyquinolines followed the first order kinetic. The first and the second order kinetic rate constant was obtained using equations 6 and 7 below:

$$-\frac{1}{t}\ln\frac{[A]}{[Ao]} = k_1(s^{-1}) \quad \text{or} \quad \frac{1}{t}\ln\frac{[Ao]}{[A]} = k_1 \tag{6}$$

$$\frac{1}{[A]} = k_2 t + \frac{1}{[Ao]} \tag{7}$$

Where $[A_o]$ is the initial mass of the metal, [A] is the mass corresponding to time t, k_1 and k_2 are the first and second order rate constant respectively (Hamadi et al., 2018).

3.4 Activation parameters

To calculate the value of activation energies and heat of adsorption, study of the effect of temperature on the corrosion of aluminium in varying HCl concentrations containing varying masses of inhibitors is of paramount important and the following Arrhenius Equations were applied:

$$CR = Aexp\left(\frac{-Ea}{RT}\right) \quad \text{(Roy et al., 1999).} \tag{8}$$

Taking logarithm of both sides at a particular temperature gives Equation 3.9, while at two different temperatures gives Equation 3.10 as follows:

$$\log(CR) = \log A - \frac{Ea}{2.303RT} \quad \text{(Roy et al., 1999)} \tag{9}$$

$$\log\left(\frac{CR_2}{CR_1}\right) = \frac{Ea}{2.303R}\left(\frac{1}{T_1} - \frac{1}{T_2}\right) \quad \text{(Roy et al., 1999)} \tag{10}$$

$$Q_{ads} = 2.303R\left[log\left(\frac{\theta_2}{1-\theta_2}\right) - log\left(\frac{\theta_1}{1-\theta_1}\right)\right] x \frac{T_1 x T_2}{T_2 - T_1} kJ/mol \tag{11}$$

Where θ_1 and θ_2 are the degrees of surface coverage at the temperatures T_1 and T_2 respectively. At constant pressure, the value of Q_{ads} approximate enthalpy of adsorption (ΔH_{ads}).

The free energy change of adsorption, ΔG^o_{ads}, is calculated usingEquation 12 (Soltani et al., 2012):

$$\Delta G^0_{ads} = - RT \ln (55.5 \times K_{ads}) \tag{12}$$

If 55.5 is the molar concentration of water in the solution, R and T remain the same as above, and Kads was obtained from the intercept of the plot of θ versus logC. For adsorption to occur, ΔGads must be negative. ΔSads is always negative because the adsorbed atoms or molecules lose degrees of freedom in the process. Therefore, ΔHads should also be negative, indicating that most adsorption processes are exothermic. In general, values of ΔG0ads near -20 kJmol-1 correspond to physisorption, while values above -40 kJmol-1 correspond to chemisorption (Soltani et al., 2012). The heat of adsorption Qads can also be defined by Equation 3.10 and depends on the energy of the bond formed between the adsorbed atom and the metal surface (Soltani et al., 2012).

The activation energy is the minimum energy required for the corrosion reaction to occur, while the heat of adsorption is the energy released when the inhibitor molecule is adsorbed on the metal surface. While the activation energy refers to the entire corrosion reaction, the heat of adsorption is specific to the interaction between the inhibitor molecule and the metal surface (Soltani et al., 2012).

Table 3: Activation Energy, E_a (kJ/mol) and Q_{ads} (kJ/mol) of Different Inhibitor Systems of 0.2, 0.4 and 0.6g/L on Aluminium at 313K and 323K Obtained through Weight Loss Method.

				6-OHQ(g/L)				
		0.00		0.2		0.4		0.6
Corrodent concentration	Ea	Qads	Ea	Qads	Ea	Qads	Ea	Qads
0.2M	63.05	0.00	19.66	-70.28	13.54	-61.01	11.03	-57.01
0.4M	58.18	0.00	20.54	-78.69	16.08	-67.66	14.97	-60.17
0.6M	43.25	0.00	22.66	-87.27	19.24	-79.81	18.46	-67.09
				7-OHQ(g/L)				
		0.00		0.2		0.4		0.6
Corrodent concentration	Ea	Qads	Ea	Qads	Ea	Qads	Ea	Qads
0.2M	63.05	0.00	12.98	-64.03	5.54	-59.99	4.17	-51.31
0.4M	58.18	0.00	17.29	-78.73	7.72	-69.35	5.31	-60.17
0.6M	43.25	0.00	19.61	-89.89	10.83	-75.63	7.78	-68.29
				8-HOQ(g/L)				
		0.00		0.2		0.4		0.6
Corrodent concentration	Ea	Qads	Ea	Qads	Ea	Qads	Ea	Qads
0.2M	63.05	0.00	20.46	-34.03	18.31	-29.99	14.98	-21.31
0.4M	58.18	0.00	21.19	-48.73	17.21	-39.35	16.08	-30.17
0.6M	43.25	0.00	23.02	-69.89	21.16	-55.63	19.64	-48.29

Table 3 shows that the activation energy decreases with increasing modifier concentration in the absence of inhibitor. This is generally consistent with chemical reaction theory, since chemical reactions occur through particle collisions. The severity of these collisions is determined by the distance between atoms (Satapathy et al., 2009). As the concentration of modifier increases, more atoms are introduced into the system, reducing the distance between atoms and requiring less energy to cause a reaction. Thus, the higher the concentration of modifier, the lower the activation energy of the corrosion reaction (Satapathy et al., 2009). The difference in activation energy and heat of adsorption with and without

inhibitor suggests that the presence of inhibitors alters the corrosion coefficient. Without the use of inhibitors, the corrosion rate is proportional to the concentration of the modifier, and no heat of adsorption is generated because the modifier does not form bonds with the metal surface (Banerjee and Saha, 2015). When inhibitors are used in Table 3, the activation energy decreases as the mass of the inhibitor increases. This indicates that the inhibitor lowers the reaction barrier and increases the corrosion rate. This may be due to the formation of unused bonds between the inhibitor and the metal surface, resulting in a lower activation energy. The increase in activation energy with increasing modifier concentration in the presence of inhibitors suggests that the inhibitor forms a barrier that makes it more difficult for the modifier to react with the metal surface. This may be due to the formation of an inhibitor atomic layer on the metal surface, preventing the modifier from reaching the surface (Seyeux et al., 2011). The increase in heat of adsorption also indicates that bonds are formed between the inhibitor and the metal surface. Table 3 shows that 7-OHQ has a lower activation energy and a higher heat of adsorption compared to the other atoms, followed by 6-OHQ and 8-OHQ, which have the highest activation energy. This may be due to the special structure of 7-OHQ, which allows it to interact with metal surfaces in a way that reduces the inhibition of the activity of the reaction.

Table 4: Enthalpy, ΔH_{ads} (kJ/mol) and Entropy, ΔS_{ads} (kJ/mol/K) Values Obtained with and without Different Inhibitors Systems of 0.2, 0.4 and 0.6g/L on Aluminium through Weight Loss Method.

				6-OHQ(g/L)				
Corrodent concentration	0.00 ΔH_{ads}	ΔS_{ads}	0.20 ΔH_{ads}	ΔS_{ads}	0.40 ΔH_{ads}	ΔS_{ads}	0.60 ΔH_{ads}	ΔS_{ads}
0.2M	32.92	0.197	25.95	0.212	22.55	0.227	17.88	0.235
0.4M	42.28	0.182	30.39	0.204	27.37	0.211	23.28	0.224
0.6M	51.77	0.167	40.55	0.187	38.48	0.199	29.87	0.207
				7-OHQ(g/L)				
Corrodent concentration	0.00 ΔH_{ads}	ΔS_{ads}	0.20 ΔH_{ads}	ΔS_{ads}	0.40 ΔH_{ads}	ΔS_{ads}	0.60 ΔH_{ads}	ΔS_{ads}
0.2M	32.92	0.197	20.54	0.209	17.55	0.224	15.38	0.229
0.4M	42.28	0.182	25.92	0.201	21.63	0.201	18.32	0.217
0.6M	51.77	0.167	30.52	0.192	31.77	0.196	23.93	0.212
				8-OHQ(g/L)				
Corrodent concentration	0.00 ΔH_{ads}	ΔS_{ads}	0.20 ΔH_{ads}	ΔS_{ads}	0.40 ΔH_{ads}	ΔS_{ads}	0.60 ΔH_{ads}	ΔS_{ads}
0.2M	32.92	0.197	25.95	0.213	23.55	0.228	19.89	0.231
0.4M	42.28	0.182	32.39	0.209	28.63	0.213	23.28	0.220
0.6M	51.77	0.167	43.52	0.189	39.47	0.198	30.87	0.211

From Table 4, we can see that as the corrosive concentration increases, the enthalpy of the system also increases. This means that the system becomes energetically more favorable for the corrosion reaction. This is because corrosives are reactants in the corrosion reaction (Shehu et al., 201). Another interesting aspect is the decrease in ΔSad with increasing corrosive concentration, since the system becomes more ordered as corrosive molecules are added. However, the opposite trend is observed for systems containing inhibitor masses. This suggests that the inhibitor hinders the corrosion reaction and lowers the energy of the system (Singh et al., 2016). The values of ΔHads and ΔSad show opposite trends as the corrosion concentration increases. This is because the inhibitors have two different effects on the system. On the one hand, they block the corrosion reaction and reduce the enthalpy of the system. On the other hand, they increase the disorder of the system and increase the entropy of the system (Singh et al., 2016). The net effect of these two opposing effects is shown in Table 4. This is an interesting example of how two opposing forces in a complex interaction can determine the overall properties of a system. The ΔHads and ΔSad values of 7-OHQ are more accurate than those of the other two inhibitors, which justifies the superiority of 7-OHQ in terms of corrosion inhibition performance.

In general, the effect of inhibitors on corrosion reactions can be summarized in two main points. First, inhibitors block the reaction and prevent the loss of metal from the surface. Secondly, the inhibitors may increase the disorder in the system and help to prevent the formation of corrosion products. The overall effect of the inhibitors is to reduce the corrosion reaction rate and prevent the damage caused by corrosion. This is very useful for practical applications where corrosion protection is important. Observations from Table 4 indicate that the differences in inhibition efficiency in Table 1 do not arise from the size of the substituents but probably from the position of the substituents. In other words, the size of the substituents attached to the quinoline does not have a significant effect on the corrosion inhibition of aluminum in HCl solution. This reflects the characteristics of a liquid or solid reaction that is likely to involve dissolution of aluminum due to insufficient inhibition (Talari et al., 2019).

Table 5: Langmuir Adsorption Isotherm Parameters Obtained from the Adsorption of the Inhibitors on Aluminium Surfaces at Different Temperatures.

		303K			313K			323K		
Inhibitor	CC	R^2	Slope	K_{ads}	R^2	Slope	K_{ads}	R^2	Slope	K_{ads}
6-OHQ	0.2MHCl	0.999	0.323	1.371	0.977	0.571	0.825	0.958	0.628	0.688
	0.4MHCl	0.993	0.403	0.830	0.997	0.412	0.777	0.964	0.459	0.683
	0.6MHCl	0.990	0.455	0.713	0.894	0.479	0.697	0.974	0.498	0.550
		303K			313K			323K		
Inhibitor	CC	R^2	Slope	K_{ads}	R^2	Slope	K_{ads}	R^2	Slope	K_{ads}
7-OHQ	0.2M HCl	0.998	0.329	0.941	0.999	0.655	0.644	0.992	0.631	0.625
	0.4M HCl	0.846	0.490	0.692	0.995	0.529	0.646	0.878	0.463	0.639
	0.6M HCl	0.972	0.315	0.833	0.996	0.510	0.599	0.997	0.636	0.428
		303K			313K			323K		
Inhibitor	CC	R^2	Slope	K_{ads}	R^2	Slope	K_{ads}	R^2	Slope	K_{ads}
8-OHQ	0.2MHCl	0.997	0.414	0.869	0.999	0.592	0.620	0.997	0.666	0.517
	0.4MHCl	0.913	0.561	0.584	0.921	0.626	0.506	0.958	0.628	0.459
	0.6MHCl	0.990	0.313	0.791	0.989	0.527	0.515	1.000	0.517	0.435

3.5 Adsorption Study

The adsorption isotherms provide valuable information on the nature of interaction between the inhibitor molecules and the metal surface. The surface coverage (θ) of the adsorbed molecules can be determined by dividing the inhibition efficiency values of the weight loss runs with 100 (Talari et al., 2019). The results obtained for surface coverage (θ) were tested using Langmuir, Temkin, Flory Huggins and El-Awardy adsorption isotherm equations as given by equations 13, 14, 15 and 16 respectively.

$$\frac{C}{\theta} = \frac{1}{K} + C \quad (13)$$

$$\theta = \frac{-\ln\log K_{ads}}{2\alpha} - \frac{\ln C}{2\alpha} \quad (14)$$

$$\log\frac{(\theta)}{C} = \log K + x\log(1-\theta) \quad (15)$$

$$\log\frac{\theta}{(1-C)} = \log K + y\log C \quad (16)$$

where C is the concentration inhibitor (g/l) and Kads is the equilibrium constant for the adsorption process. The parameters of the Langmuir adsorption isotherm are given in Table 3.5. The linear regression coefficients were close to 1 for almost all inhibitors and the data used to plot the isotherms were the surface coverage θ at various concentrations of selected quinolines at 303 and 323 K. The data were tested using various adsorption isotherm equations, namely Langmuir, Temkin, Flory-Huggins and El-Awady, showing the linearization parameters for each adsorption model (Talari et al., 2019). For Langmuir, the values of the regression coefficient R2 for all three systems were mostly greater than 1, therefore the surface coverage determined from the IE% values fits all the adsorption models (Talari et al., 2019). However, the Langmuir adsorption isotherm was the best fit, as almost all systems had R2 values close to 1. In some cases, it may be sufficient to confirm the adsorption of the inhibitor using data fitted to the isotherm, and it is often desirable to extend the scope to include the derivation of thermodynamic parameters related to the adsorption process, using the relationship between the adsorption equilibrium constant (kads) and the standard adsorption free energy ΔGads (Talbot et al., 2018).

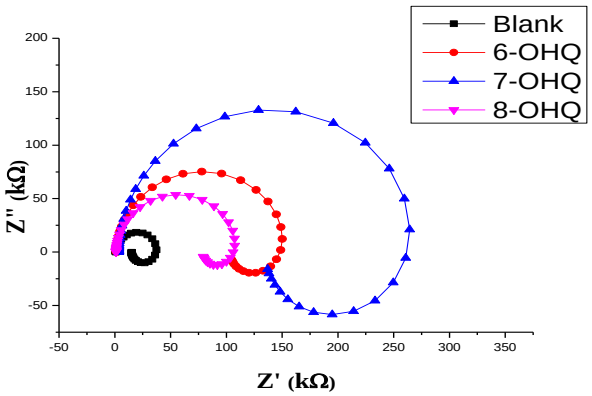

Figure 15: Impedence responses at the metal/acid interface for the corrosion of aluminium in the absence and in the presence of 0.4g/L 6-OHQ, 7-OHQ and 8-OHQ inhibitors in 0.4M HCl at 303k.

The figures 15 depict the characteristics impedance responses at the metal/acid interface for the corrosion of aluminium in the absence and in the presence of 0.4g/L each inhibitor in 0.4M HCl. The impedance spectra for the Nyquist plots of aluminium in the acid solutions in the absence and presence of the hydroxyquinolines were appropriately analyzed by fitting to the equivalent circuit model Rs (C_{dl} Rct), which has been previously used to model the metal/acid interface (Verma et al., 2016; Chen et al., 2018).

Table 6: Impedance data for the corrosion of aluminium in 0.4 M HCl in the absence and presence of 0.4g/L Inhibitor for each system at 303 K

System	R_{ct} (Ω cm²)	C_{dl} (μΩ⁻¹Sⁿcm⁻²)	N	IE%
HCl (Blank)	134.5	3.56	0.86	0.00
6-OHQ	186.6	2.21	0.96	46.16
7-OHQ	1021.6	1.74	0.93	75.82
8-OHQ	252.7	2.71	0.92	18.23

The corresponding impedance parameters are given in Table 6. The increase in Rct values in the inhibited systems, i.e. the increase in the diameter of the Nyquist semicircle and the corresponding decrease in the double layer capacitance (Cdl), confirms the anticorrosive properties of quinoline. The observed decrease in Cdl values, which usually corresponds to a change in the double layer thickness, can be attributed to the adsorption of quinoline (which has a lower dielectric constant compared to the displaced adsorbed water molecules) at the metal/acid interface, thereby positioning the metal against the corrosive action of aggressive acids. However, 7-OHQ has the largest amplitude among the three hydroxyquinolines tested, as shown in Figure 15, and also the highest percent inhibition efficiency, as shown in Table 6, further supporting its superiority in corrosion inhibition compared to 6-OHQ and 8-OHQ. The amplitude of the Nyquist plot, the magnitude and trend of the achieved inhibition efficiency %IE are consistent with those obtained from weight loss measurements.

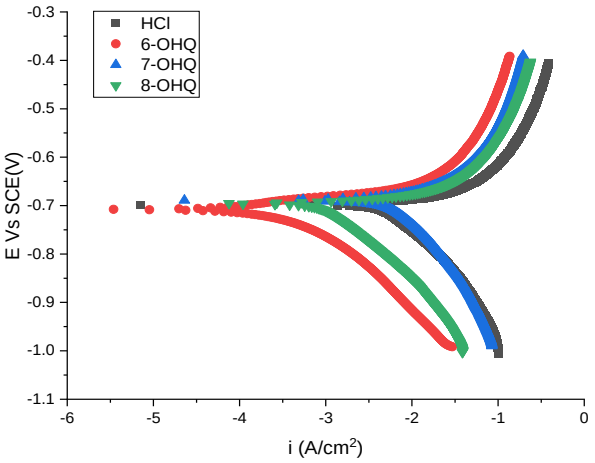

Figure 16: Polarization at the metal/acid interface for the corrosion of aluminium in the absence and in the presence of 0.4g/L 6-OHQ, 7-OHQ and 8-OHQ inhibitors in 0.4M HCl at 303k.

From Table 7, it is clear that the insertion of aluminum at a concentration of 0.4 M in the corroding solution (HCl) without the use of inhibitors results in high values of both icorr and corrosion rate at room temperature, whereas these tend to decrease when inhibitors are used. When 0.4 g/L 6-OHQ (6-hydroxyquinoline) is introduced into the corroding solution, it causes some inhibition. In the first system with 0.4 g/L 6-OHQ (6-hydroxyquinoline), the icorr value decreased from 17.20 μA to 600.00 μA, and the achieved corrosion rate and inhibition efficiency were 385 mPy and 42.16%, respectively.

Potentiodynamic polarization diagrams show that the inhibitors affect both the anodic metal dissolution and the cathodic hydrogen evolution reaction (Chen et al., 2018). For some of the inhibitors used, the cathodic Tafel lines are parallel for all inhibitors, indicating that the inhibitor molecules only slightly change the cathodic hydrogen evolution reaction (Talbot, and Talbot, 2018).

Table 7: Potentiodynamic polarization data for the corrosion of aluminium in 0.4 M HCl in the absence and presence of 0.4g/L Inhibitor for each system at 303 K.

System	BetaA(V/d)	BetaC(V/d)	i_{corr}(μA)	E_{corr}(mV)	CR (mpy)	%IE
Blank	188.2e-3	414.2e-3	617.20	-998.0	11.02e3	0.00
6-OHQ	121.6e-3	170.8e-3	600.00	-701.00	185.40	42.16
7-OHQ	32.9e-3	219.8e-3	129.00	-689.00	18.65e3	69.52
8-OHQ	88.30e-3	345.2e-3	292.00	-779.00	187.40	28.23

The corrosion potential values (Ecorr) in Table 7 show that the addition of inhibitors shifts the corrosion potential to a positive direction. If the corrosion potential changes significantly with the addition of inhibitors, the inhibitor is believed to work by blocking active sites. On the other hand, a negligible change in Ecorr with the addition of inhibitors suggests that the inhibitors act through a geometric blocking effect (Chen et al., 2018). Thus, inhibitors in these systems are believed to work by blocking active sites. Table 7 also shows that the addition of inhibitors decreases the Icorr values, while it increases the Ecorr values. This trend of increasing Ecorr while decreasing Icorr indicates increased corrosion inhibition and surface hydrophobicity, which can be attributed to inhibitor molecules adsorbed on the aluminum surface. In this study, the maximum change in Ecorr due to the addition of inhibitors was mostly below 45 mV, suggesting that the inhibitors indeed act as a mixed type, since both cathodic and anodic processes are affected (Verma et al., 2016).

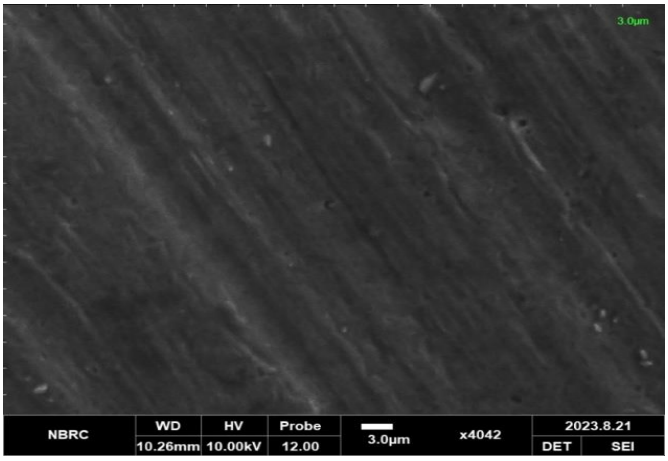

Figure 17: Micrograph of the Raw Aluminium image prior to corrosion study.

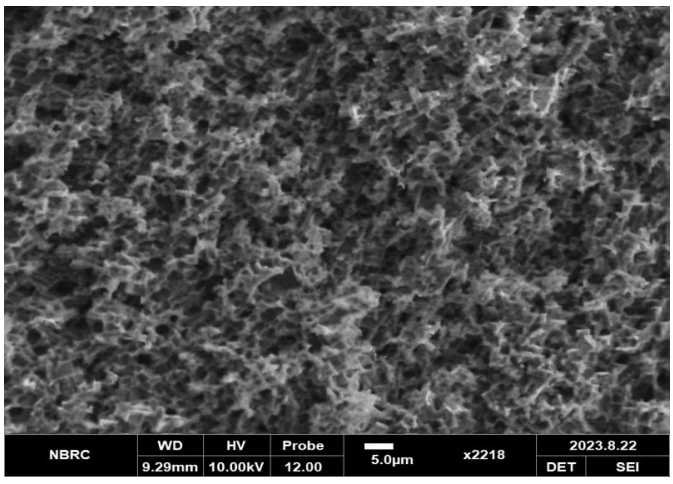

Figure 18: Micrographs of Aluminium after dipping in 0.4M HCl for 5 hour without inhibitor.

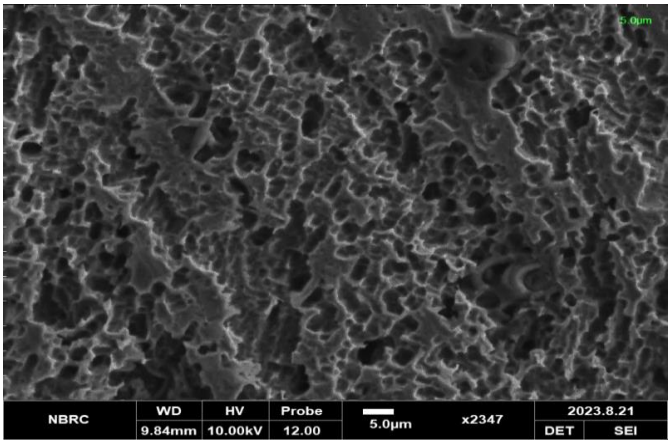

Figure 19: Micrographs of Aluminium after dipping in 0.4M HCl for 5 hour with 0.4g/L 6-OHQ inhibitor.

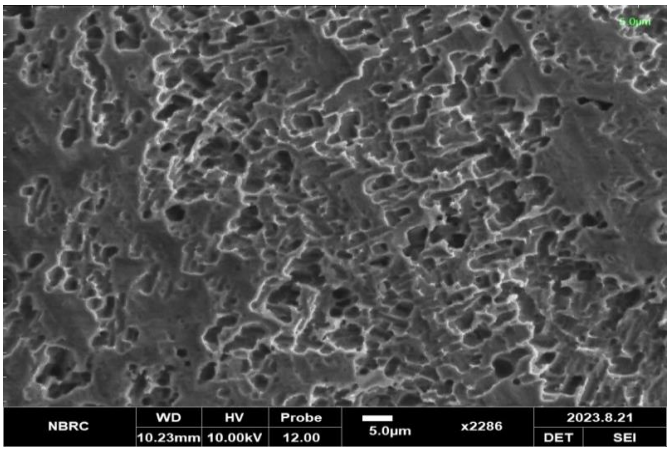

Figure 20: Micrographs of Aluminium after dipping in 0.4M HCl for 5 hour with 0.4g/L 7-OHQ inhibitor.

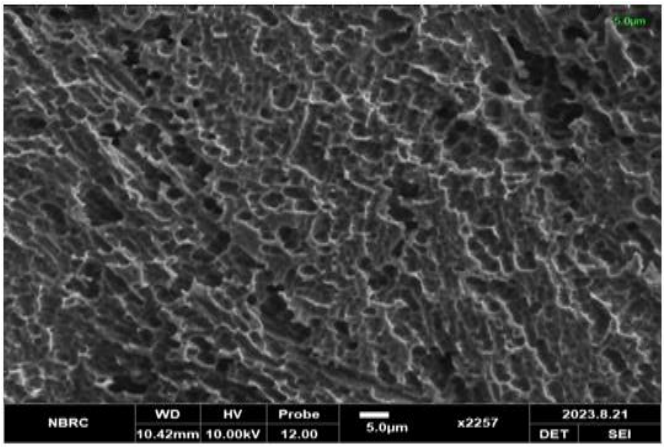

Figure 21: Micrographs of Aluminium after dipping in 0.4M HCl for 5 hour with 0.4g/L 8-OHQ inhibitor.

Figure 17 shows the surface morphology of aluminum before the corrosion test, showing a smooth and transparent surface. Figure 18 shows a microscopic image of this surface after immersion in 0.4 M HCl solution without inhibitors. After 5 hours of immersion, corrosion marks are clearly visible on the surface, indicating the influence of an aggressive environment. Figures 19, 20 and 21 show microscopic pictures of samples immersed in 0.4 M solutions of the respective inhibitors. It can be clearly seen that all samples immersed in the medium containing the inhibitors have a thick layer consisting of corrosion products and inhibitor molecule deposits. In the unprotected samples, more pitting can be seen to have formed. With the addition of inhibitors, the surface becomes hydrophobic, which also confirms the adsorption of quinoline molecules on the aluminum surface and the formation of a protective surface film, as is typical for mixed inhibitors (Verma et al., 2016). However, Figure 20 shows the surface with 7-OHQ inhibitor, which shows a thicker layer on the aluminum-protected surface. This means that it has better corrosion resistance than other tension inhibitors, which is consistent with the weight loss and electrochemical experiments.

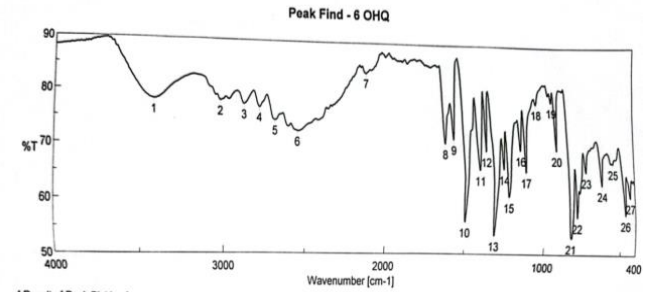

[Result of Peak Picking]

No.	Position	Intensity	No.	Position	Intensity	No.	Position	Intensity
1	3411.46	78.0404	2	3014.19	77.9589	3	2871.49	77.3638
4	2778.92	76.8654	5	2684.43	74.4865	6	2547.5	72.4918
7	2119.39	83.875	8	1633.41	70.4046	9	1579.41	71.2373
10	1500.35	55.9915	11	1415.49	65.5234	12	1375	69.0808
13	1317.14	53.4794	14	1265.07	65.7537	15	1232.29	60.6537
16	1157.08	69.3324	17	1124.3	65.2972	18	1047.16	78.3797
19	944.949	78.8283	20	919.879	69.5015	21	823.455	53.0523
22	788.743	56.9487	23	727.032	65.5172	24	620.966	63.0748
25	541.899	67.4007	26	466.689	57.5135	27	431.977	60.8542

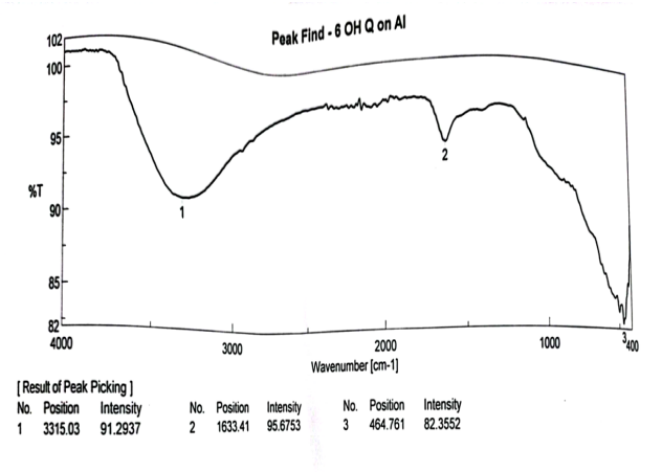

Figure 22: FTIR spectra of Aluminium corrosion products after immersion in 0.4MHCl with and without 0.4g/L 6-OHQ at 303K

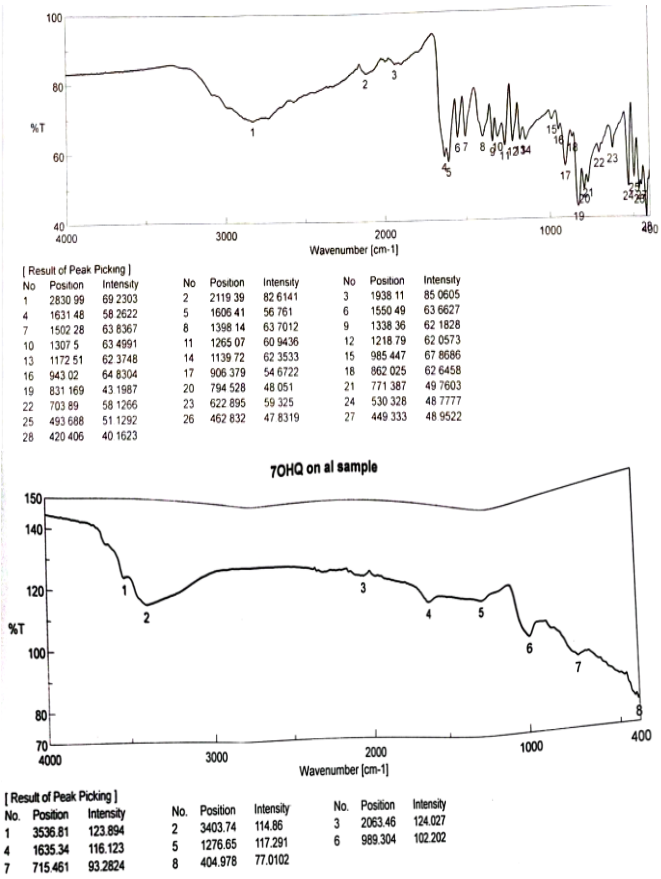

Figure 23: FTIR spectra of Aluminium corrosion products after immersion in 0.4MHCl with and without 0.4g/L 7-OHQ at 303K

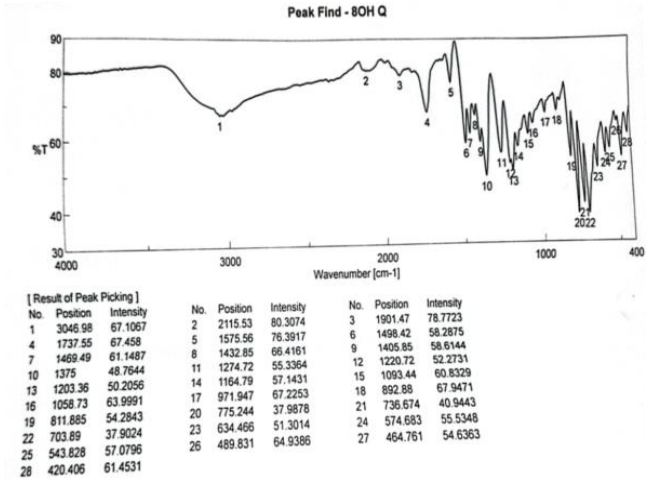

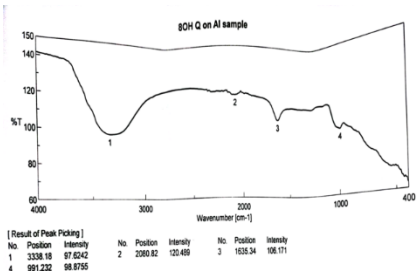

Figure 24: FTIR spectra of Aluminium corrosion products after immersion in 0.4MHCl with and without 0.4g/L 8-OHQ at 303K

3.6 Fourier Transform IR Analysis

FTIR spectra of hydroxyquinoline derivatives on aluminum surfaces are shown in figures 22, 23 and 24 for 6-OHQ, 7-OHQ and 8-OHQ, respectively.

The appearance of a strong peak at about 3500 cm-1 is due to the hydroxyl group, the peak at about 1615 cm-1 corresponds to the aromatic nucleus, the nitrogen atom in the molecule has a peak at about 1423 cm-1, the peak at about 1500 cm-1 is located at the carbon-carbon double bond, and the peak of the carboxyl group generally appears at 1700 cm-1 for all hydroxyquinoline molecules. A concentration of 0.4 g/L hydroxyquinoline in 0.4 MHCl without the addition of aluminum foil clearly showed the presence of hydroxyl groups (OH), aromatic rings, nitrogen, carbon-carbon double bonds, and carboxyl groups. However, when aluminum is added to the solution, the peak corresponding to the OH relaxation at 3510 cm-1 shifts to 3500 cm-1 for 6-OHQ and 8-OHQ, and to about 3.496 cm-1 for 7-OHQ molecules. The aromatic ring at 1.615 cm-1 shifts to 1513 cm-1, and the nitrogen peak that appeared at about 1423 cm-1 shifts to 1435 cm-1 and disappears in the 7-OHQ molecule. These changes are believed to be due to the interaction of the hydroxyquinoline molecule with the metal surface.The high O-H and nitrogen stretching values, and more importantly the disappearance of the N peak for 7-OHQ, are evidence that the aluminum surface is binding to the hydroxyquinoline molecule. This confirms the fact that the mechanism is both physical and chemical adsorption (Chen et al., 2018).

3.7 Mechanism of Inhibition

Naturally, before investigating corrosion by oxidation, an air-passivating film of aluminum oxide is formed on the surface of the test aluminum plate, as shown in equation (17):

$$4Al + nH_2O + 3O_2 \rightarrow 2Al_2O_3(H_2O)n \quad (17)$$

However, the dissolution of aluminum in aggressive media (acidic solutions) can be shown by equation (18)

$$Al \rightarrow Al^{3+} + 3^{e-} \quad (18)$$

Die QuinolineThe derivatives 6-OHQ, 7-OHQ, and 8-OHQ used here have the same molecular weight and similar structure. The interaction of aluminum with these molecules generally involves the formation of a complex between the aluminum ion and the oxygen and nitrogen atoms of the hydroxyquinoline molecule. This complex is hydrophobic and acts as a corrosion inhibitor by blocking active sites on the aluminum surface, preventing reactions between aluminum and the corrosive medium. The most likely chemical equation for this interaction is shown in equation (19):

$$Al^{3+} + 3C_9H_6NO + 6H_2O \rightarrow [Al(C_9H_6NO)_3]^{3+} + 6OH^- \quad (19)$$

The aluminum ion (Al3+) forms a complex with three molecules of hydroxyquinoline and six molecules of water to form a hydrophobic product. Furthermore, based on the FTIR peaks, the difference in inhibition efficiency of molecules despite having the same mass and structure is likely due to the alignment of the positions of the substituents (OH) on the parent quinoline molecule. It has been suggested that intramolecular hydrogen bonding occurs in 8-OHQ, resulting in insufficient donation of free electrons from the hydroxyl group in the formation of metal complexes. This leads to poorer inhibition performance. The stronger the intramolecular hydrogen bonding, the slower the complex formation and the lower the inhibition efficiency. At the 7-position, the OH group probably does not form an intramolecular hydrogen bond.

4. Conclusion

The effect of the position of the hydroxyl substituent on quinoline used as

an aluminum corrosion inhibitor in hydrochloric acid has been well studied experimentally. Among the three hydroxyquinoline substituents (6-hydroxyquinoline, 7-hydroxyquinoline, and 8-hydroxyquinoline), 7-hydroxyquinoline showed the highest anticorrosion performance under all conditions. The results of mass loss, energy potential polarization, and impedance measurements confirmed these observations. The position of the hydroxyl substituent on the quinoline particles seems to have some effect on the anticorrosion performance of aluminum in acidic environments, as shown by the test results of mass loss, EIS, and PDP. Examination of electron microscope images confirmed that 7-OHQ more reliably blocked the corrosion sites of the acidic aluminum plate. This indicates that 7-OHQ is an effective corrosion inhibitor since it forms stronger bonds with metal surfaces and reduces the activation energy of the corrosion reaction. This suggests that 7-OHQ may be a promising candidate for use in mechanical applications where corrosion protection is required. According to FTIR, significant changes in wavenumbers are due to the interaction of hydroxyquinoline particles with the metal surface. The high distortion values of the hydroxyl and nitrogen peaks observed with 7-OHQ, as well as the disappearance of the N peak, are evidence of the binding of the aluminum surface to the hydroxyquinoline atoms. This is confirmed by the combined adsorption apparatus.

REFERENCE

Abdallah, M., 2002. drugs of Rhodamine Azosulpha as corrosion inhibitors for corrosion of 304 Stainless steel in hydrochloric acid solution arrangement, Journal of Corrosion Science, Vol. 44; Pp. 717-728.

Ali, G, Sayed, Ashraf, M., Ashmawy, and Deyab, M.A., 2023. Union, depiction and application of modern erosion inhibitors for CS AISI1095 in 1.0MHCl based on Benzo quinoline subsidiaries, Journal of Logical Reports, Vol. 13 (13761)

Awad, M.K., 2004. Investigation of the inhibition efficiency of thiourea derivatives as corrosion inhibitors by Semiempirical method, Journal of elctroanalytical chemistry,567: Pp. 219– 225.

Babic´ Samardz˘ija, K., Khaled, K.F., and Hackerman, N., 2005a. Investigation of the inhibitingaction of O,S and Ndithiocarbamato(1,4,8,11tetraazacyclotetradecane) cobalt(III) complexes on the corrosion of iron in $HClO_4$ acid, Applied Surface Science 240, Pp. 327–340.

Babic-Samardz, ija, K., and Hackerman, N., 2006. Iron corrosion inhibition using dihydrobi and hydrotris (1-pyrazolyl) borates, Anti-corrosion Method and Material, 53 : Pp. 19– 29.

Banerjee, P., and Saha, S.K., 2015. Theoretical approach to understanding of the inhibition mechanism of steel corrosion with two amino-benzonitrile inhibitors. Research in Science Advance.; 5(87):71120.

Chen, Y., Zhang, H., and Zhang, Z., 2018. Comparative studies of two benzaldehyde thiosemicarbazone derivatives as corrosion inhibitors for mild steel in 1.0 M hydrochloric acid solution, Result Phys. Vol. 11, Pp. 554-563, https://doi.org/10 .1016/j.rinp..09.038.

Chi, M., and Zhao, Y.P., 2009. Adsorption of formaldehyde molecule on the intrinsic and Al-doped grapheme: A first principle study, Computational Materials Science, 48: Pp. 1085–1090.

Cicek, and Al-Numan, B., 2011. Corrosion Chemistry. United States of America: Scrivener Publishing LLC and Wiley and Sons, 2011, Pp. 7–14.

Dai, W., and Zhang, Y.Y., 2012. Molecular dynamics simulation of the adsorption behaviour of amino acid corrosion inhibitor on Cu (1 0 0) surface. Applied Mechanics and Materials, 121-126: Pp. 226-230.

Dai, W., and Zhang, Y.Y., 2012. Molecular dynamics simulation of the adsorption behaviour of amino acid corrosion inhibitor on Cu (100) surface. Applied Mechanics and Materials, 121-126: Pp. 226-230.

Dakeshwar, K., Verma, A., Jeenat, A., and Mumtaz A. Q., 2021. Computational Modeling:Hypothetical Prescient Devices for Planning of Potential Natural Erosion Inhibitors, Diary of Atomic Structure, Vol. 1236:
130294

Eddy, N.O., Odoemelam, S.A., and Odiongenyi, A.O., 2009. Inhibition, adsorption and synergistic studies on ethanol extract of Gnetum africana as green corrosion inhibitor for mild steel in sulphuric acid", Green Chemistry Letters and Re views,2(2): Pp. 111-119.

EI-Awady A. A., AbdeI-Nabey B.A., and Aziz, S.G., 1994. Engine, thermodynamic and adsorption isotherms examinations for the restriction of the destructive disintegration of steel by cyclic and open-chain amines, Diary of the Electrochemical Society, 139(8):Pp. -2154.

Ekanem, U.F., Umoren, S.A., Udousoro I.I. and Udoh, A.P., 2010. Inhibition of gentle steel corrosion in Hydrochloric acid environment, utilizing pineapple takes off (Ananas comosus L.) extricate (survey), Journal of Materials Science; 65(26):Pp. 5558-5566.

Elfaydy, M., Lgaz, H., Salghi, R., Larouj, M., Jodeh, S., Rbaa, M., Oudda, H., Toumiat, K., and Lakhrissi, B., 2016. Investigation of corrosion inhibition mechanism of quiniline Derivative on Mild steel in HCl Solution" : Experimental, Theoretical and Monte Carlo simulation, Journal of material and Environmental Science. Vol. 7(9) 3193-3210, ISSN: Pp. 2028-25086.

El-HassanAssiri, M., Driouch, J. L-Z., Bensouda A. E. M. S., 2020. Development and validation of QSPR models for corrosion inhibition of carbon steel by some pyridazine derivatives in acidic medium, Heliyon, Vol.15, Pp. 50-67

Hamadi, L., Mansouri, S., Oulmi, K., and Kereche, A., 2018. The use of amino acids as corrosion inhibitors for metals: A review, Egyptian Journal of Petroleum, vol. 27, no. 4, Pp. 1157–1165.

Kadapparambil S., Kavita Y., Manivannan, R., and Noyel, V. S., 2017. Electrochemical investigation of the corrosion inhibition mechanism of Tectona grandis leaf extract for SS304 stainless steel in hydrochloric acid, De Gruyter, DOI 10.1515/corrrev-2016-0074

Khaled, K.F., and Abdel Shafi, N. S., 2011. Study of Corrosion Inhibitors by QSAR Modeling: Genetic Function Approximation and Molecular Dynamics Simulation Methods, International Journal Of Electrochemical Science, Vol.6 Pp. 4077 - 4094

Kiani, M. A., Mousavi, M. F., Ghasemi, S., Shamsipur, M., and Kazemi, S. H., 2008. Inhibition effect of some amino acids on corrosion of Pb-Ca-Sn alloy in sulphuric acid solution. Corrosion Science, 50: Pp. 1035-1045.

Kikuchi, O., 1987. Systematic QSAR procedures with quantum chemical descriptors, Vol. 6: Pp. 179–184.

Kliskic, M., Radoservic, J., Gudic, S., and Katalinic, V., 2000. Aqueous extract of Rosm marius officinalis L. as inhibitor of Al-Mg alloy corrosion in HCl solution. Journal of Applied Electrochemistry 30: Pp. 823-830.

Larif, M., Chtita, S., and Adad, A., 2013. Predicting biological activity of Anticancer Molecules 3-ary l-4-hydroxyquinolin-2-(1H)-one by DFT-QSAR models. Int J.;Vol. 3(12):Pp. 32.

Li, N., Dong, C., Man, C., Yao, J., 2019. InSitu Electrochemical Atomic Force Microscopy and Auger Electro Spectroscopy Study on the Passive Film Structure of 2024-T3 Aluminium Alloy Combined with a Density Functional Theory Calculation, Advance Engineering. Material. 21 1900386. doi.org/10.1002/adem.201900386.

Moussa, M. N., Fouda, A. S., Taha, F. I., and Eluenna, A., 1988. Comparative studies of aluminium corrosion in HCl medium using organic inhibitor, Bull Korean Chemical Society, 9(4) 191. s

Murulana, L.C., Singh, A.K., and Shukla, S.K., 2012. Experimental and quantum chemical studies of some bis (trifluoromethyl-sulfonyl) imideimidazolium based ionic liquids as corrosion inhibitors for mild steel in HCl solution. Ind Eng Chem Res.;51(40):13282. DOI: https://doi.org/10.1021/ie300977d

Olufunmilayo, O. J., and Olakunle O. J., 2020. Corrosion Inhibition of Aluminium Alloy through Chemical Inhibitors: An Overview of Conference Series; Materials Science and Engineering, Volume 1107, Pp. 345-619

Qiang, Y., Zhang, S., Tan, and Chen, S., 2018. Evaluation of Ginkgo leaf extract as an eco-friendly corrosion inhibitor of X70 steel in HCl solution, Corrosion Science, vol. 133, Pp. 6–18.

Roy, R.K., Pal, S., Hirao, K., 1999. On non-negativity of Fukui function indices, J. Chem. Phys. 110 8236-8245, https://doi.org/10.1063/1.478792.

Satapathy, A.K., Gunasekaran, G., Sahoo, S. C., Amit, K., and Rodriquez, P. V., 2009. Corrosion inhibition by Justicia gendarussa plant extract in hydrochloric acid solution," Corrosion Science, vol. 51, no. 12, Pp.

2848–2856.

Seyeux, S., Frankel, G.S., Missert, N., Unocic, K.A., Klein, L.H., Galtayries, A., Marcus, P., 2011. ToF-SIMS Imaging Study of the Early Stages of Corrosion in Al-Cu Thin Films, Journal of Electrochemistry, 158 C165–C171. https://doi.org/10. 1149/1. 3568944.

Shehu, U., Najib, U. I., Gaya and Muhammad, A. A., 2019. Influence of Side Chain on the Inhibition of Aluminium Corrosion in HCl by α-Amino Acids, King Mongkut's University of Technology North Bangkok.

Singh, P., benso, E. E., and Olasunkanmi, L. O., 2016. Experimental, theoretical, and surface morphology studies of corrosion inhibition effect of green naphthyridine derivatives on mild steel in hydrochloric acid solution, Journal of Physical Chemistry.;Vol. (6): Pp. 3408. DOI: https://doi.org/10.1021/acs.jpcc.5b11901

Soltani, N., Tavakkoli, M., Khayatkashani, and Jalali, M. R., 2012. Green approach to corrosion inhibition of 304 stainless steel in hydrochloric acid solution by the extract of Salvia officinalis leaves, Corrosion Science, vol. 62, no. Pp. 122–135.

Talari, M., Nezhad, S.M., Alavi, S.J., Mohtashamipour, M., Davoodi, A., Hosseinpour, S., 2019. Experimental and computational chemistry studies of two imidazole-based compounds as corrosion inhibitors for mild steel in HCl solution, J. Mol. Liq. 286 110915, https://doi.org/10.1016/j.molliq.2019. 110915.

Talbot, D.E.J., and Talbot, J. D. R., 2018. Corrosion Science and Technology, 3rd ed. New York: Taylor and Francis, Pp. 159–194.

Verma, C., Olasunkanmi, L.O., and Ebenso, E.E., 2016. Adsorption behavior of glucosamine-based, pyrimidine-fused heterocycles as green corrosion inhibitors for mild steel: experimental and theoretical studies. Journal Physical Chemistry.;Vol. 120(21):11598. DOI: https://doi.org/10.1021/acs.jpcc.6b04429